RSC Advances

PAPER

View Article Online
View Journal | View Issue

Cite this: *RSC Adv.*, 2024, **14**, 39102

Antitumor activity of bimetallic silver/gold nanoparticles against MCF-7 breast cancer cells†

Juan J. Martínez-Sanmiguel, *[a] Diana Zarate-Triviño,[b] María Paula García-García,[a] José Miguel García-Martín, [c] Álvaro Mayoral, [d] Yves Huttel, [e] Lidia Martínez [e] and Jorge L. Cholula-Díaz *[a]

Breast cancer poses a global threat with rising incidence and high mortality. Conventional treatments, including chemotherapy, radiation, surgery, and immunotherapy, have side effects, such as resistance issues and adverse effects due to genetic mutations. Meanwhile, noble metal nanoparticles (NPs) synthesized using environmentally friendly methods offer alternative treatments. Bimetallic gold (Au) and silver (Ag) NPs, using natural compounds like starch as stabilizers, enhance biomedical applications, including breast cancer therapies. In this work, the optical properties, stability, and particle size of colloidal bimetallic Ag/Au NPs were analyzed using UV-visible spectroscopy and ζ-potential measurements. The structural properties of the NPs were studied by powder X-ray diffraction (PXRD), while the morphology, chemical composition and particle size were determined using scanning transmission electron microscopy (STEM). The antitumor properties of the Ag/Au NPs were analyzed on human breast cancer cells (MCF-7) using the MTT viability method, reactive oxygen species (ROS) production, and genotoxicity assays. Peripheral blood mononuclear cells (PBMCs) were used as a reference of healthy cells. UV-vis spectroscopy and EDX mapping analysis confirmed the synthesis of bimetallic Ag/Au NPs. Localized surface plasmon resonance (LSPR) absorption bands shifted from 407 nm (Ag) to 524 nm (Au) based on the chemical composition of the NPs. The Ag/Au NPs showed cytocompatibility in PBMCs and a dose-dependent anticancer effect against MCF-7 cancer cells, as well as cell death dependent on ROS production was observed, particularly in NPs with atomic compositions of 50 and 75 at% Ag. This biological activity of the bimetallic NPs was associated with genotoxic damage of 20–24% greater than that observed in the monometallic counterparts. This study demonstrated the synthesis of mono- and bimetallic Ag/Au NPs using a rapid, reproducible and environmentally friendly method, with successful biomedical application against human breast cancer MCF-7 cells.

Received 29th August 2024
Accepted 27th October 2024

DOI: 10.1039/d4ra06227b

rsc.li/rsc-advances

1 Introduction

Breast cancer has emerged as one of the foremost threats to women's health worldwide, representing a medically and scientifically daunting challenge of alarming proportions. With a growing occurrence, mainly in countries with high levels of development, an estimated incidence rate of more than 70/100 000 (ref. 1–5) and substantial mortality rates, for instance, there were estimated 685 000 female deaths worldwide in 2022. Despite the advances in understanding the underlying mechanisms of breast cancer and the development of conventional therapies, significant limitations persist in the effectiveness of current treatments.[6,7]

Traditional therapeutic approaches, such as chemotherapy and radiation therapy, often entail adverse side effects and limited efficacy.[8] Breast cancer shows multiple mutations that result in constant cell proliferation and evasion of regulated cell death (RCD), a process by which the cell initiates its mechanisms to self-destruct.[9] The first-line therapies for breast cancer consist of surgery, immunotherapy, polyamine synthesis inhibitors, individual micronutrient supplementation, hormonal therapy, chemotherapy, and radiotherapy.[10,11] However, these treatments also cause many side effects. Moreover, it is known that mutations or deletions in proteins related to apoptosis induce resistance to conventional treatments.[12]

[a]*School of Engineering and Sciences, Tecnológico de Monterrey, Av. Eugenio Garza Sada 2501, Monterrey 64849, N.L., Mexico. E-mail: jorgeluis.cholula@tec.mx; Tel: +52 8183582000*

[b]*Laboratorio de Inmunología y Virología, Facultad de Ciencias Biológicas, Universidad Autónoma de Nuevo León, San Nicolas de los Garza, Nuevo León, 66455, Mexico*

[c]*Instituto de Micro y Nanotecnología (IMN-CNM), CSIC (CEI UAM+CSIC), Isaac Newton 8, 28760 Tres Cantos, Spain*

[d]*Instituto de Nanociencia y Materiales de Aragón (INMA), CSIC-Universidad de Zaragoza, Pedro Cerbuna, 50009 Zaragoza, Spain*

[e]*Instituto de Ciencia de Materiales de Madrid (ICMM), CSIC, Sor Juana Inés de la Cruz 3, 28049 Madrid, Spain*

† Electronic supplementary information (ESI) available. See DOI: https://doi.org/10.1039/d4ra06227b

In this context, nanotechnology emerges as a promising field for revolutionizing cancer treatment, with a particular focus on the application of noble metal nanoparticles (NPs). The significance of these nanoparticles in the field of medicine is underscored by their essential chemical and physical properties, including size and atomic composition.[13] Nowadays, nanotechnology provides innovative options to counteract cancer diseases in the treatment of breast cancer, such as the use of NPs for (1) drug delivery, either targeted administration or combination therapies, incorporating chemotherapy, gene therapy and immunotherapy within a single nanoparticle;[14,15] (2) magnetic hyperthermia;[16] (3) imaging and diagnosis[17] and (4) immunotherapy benefits from nanovaccines and localized administration of immunomodulators among others. These various strategies show the potential of nanotechnology to improve breast cancer treatment.[18,19]

As nanotechnology showcases its potential in diverse strategies for breast cancer treatment using monometallic NPs, the exploration extends to bimetallic nanomaterials broadening the spectrum of possibilities for combating breast cancer and other malignancies.[20–23] Bimetallic nanomaterials are of considerable interest due to their chemical stability and their unique properties. Some common combinations include the use of noble metals, such as Ag, Au, Pt and Pd. These metals can be combined to enhance their applications in the biomedical field. In this regard, antitumor activity of bimetallic noble metal NPs has been documented in several studies against different types of cancer, including breast cancer cells.[24–27] For example, Pt/Pd NPs shown activity against lung cancer (A549) and breast adenocarcinoma (MCF-7) with a CC_{50} of 8.8 g mL^{-1} and 3.6 g mL^{-1}, respectively.[27] Ag/Cu NPs showed strong activity against breast cancer (MDA-MB-231), where CC_{50} values calculated after 24 h of incubation were 19.27 μg mL^{-1}.[26] In the case of Ag/Au NPs, HepG2 (liver cancer), MDA-MB-231 and MCF-7 have been reported.[24,25] The anticancer activity of these bimetallic nanostructures relies on their particle size and dose, as well as the synergistic effect between the two metals that form the individual nanocrystals.[28] Furthermore, an important factor in cell death processes is oxidative stress that is originated when there is an increase in the production of free radicals and reactive oxygen species (ROS).[29,30] ROS are byproducts of aerobic metabolism in mitochondria that have inherent chemical properties that confer reactivity to different biological targets. High concentrations of ROS in the cell lead to cell death,[29] normally associated with oxidative stress, inducing pathologies by generating damage to lipids, proteins, and DNA.[31] In several reports, it has been shown that different types of NPs can induce an increase in ROS production in the cell and ultimately leading to cell death.[32] Such is the case of Ag/Au NPs coated with polydopamine, which showed antitumor properties against bladder cancer (T24), establishing a death mechanism related to the production of ROS.[33] Our previous study demonstrated that combination of both Ag and Au in a single NP coated with starch confers advantageous biological activities against melanoma cells, distinguishing between healthy human fibroblast cells.[34]

As the exploration of innovative solutions in breast cancer treatment continues, the intersection of nanotechnology and green principles becomes increasingly relevant. This approach not only aligns with sustainable practices but also underscores the potential of green nanotechnology in biomedical applications. Hence, the purpose of this study was to evaluate the cytotoxicity of starch-stabilized Ag/Au NPs against the human breast cancer MCF-7 cell line, and their cytocompatibility in peripheral blood mononuclear cells (PBMCs), as a healthy cell model. In addition, it was confirmed that cell death was related to the production of ROS after treatment with the Ag/Au NPs. Additionally, it was shown that the bimetallic NPs with a higher Ag atomic composition produce a greater DNA damage than the monometallic counterparts.

2 Experimental section

2.1 Synthesis of Ag/Au NPs

Silver nitrate ($AgNO_3$) was purchased from Thermo Fisher Scientific (Waltham, MA, USA), sodium tetrachloroaurate ($NaAuCl_4$) was purchased from Sigma-Aldrich Co. (St Louis, MO, USA), sodium hydroxide (NaOH) and soluble starch was purchased from Fermont (Monterrey, Mexico). The mono- and bimetallic Ag/Au NPs were synthesized based on a method reported previously.[34] First, a 1% w/v aqueous starch solution was heated under constant reflux and stirred for 30 min. For the synthesis of Ag/Au NPs, 9.5 mL of deionized water were heated to 70 ± 2 °C, afterwards the starch solution was added and then the NaOH. Subsequently, Au and/or Ag precursors were added as described in Table 1. The reaction mixture was heated in a water bath at 70 °C for 2 h. Subsequently, the samples were centrifuged using a 0.2 μm filter. From now on, the samples are called according to their atomic composition (*i.e.*, Ag75% – Au25% is Ag75), as described in Table 1.

2.2 Characterization of the Ag/Au NPs

2.2.1 UV-vis spectroscopy. UV-visible absorption spectra were obtained using a PerkinElmer 365 spectrometer (PerkinElmer Inc., Waltham, MA, USA). Absorption spectra were measured in the range of 300–800 nm with a speed scan of 20 nm min^{-1} and a scan step of 0.5 nm. The noble metal NP colloids were diluted at a 1 : 5 ratio with deionized water to measure their absorption spectra.

2.2.2 Powder X-ray diffraction. Powder X-ray diffraction (PXRD) measurements of the nanoparticles were performed using a MiniFlex 600 diffractometer (Rigaku, Tokio, Japan) operating at 40 kV and 15 mA with Cu Kα ($\lambda = 1.542$ Å) radiation.

Table 1 Experimental parameters used in the synthesis of colloidal Ag/Au NPs

Nanosystem	1% (w/v) starch solution (μL)	25 mM $AgNO_3$ (μL)	25 mM $NaAuCl_4$ (μL)
Ag	500	250	0
Ag75	500	375	125
Ag50	500	250	250
Ag25	500	125	375
Au	500	0	250

The data were collected over the 2θ range from 10 to 80° with a step size of 0.05° intervals with a counting time of 0.6 s at each step. The PXRD samples were prepared by drying 10 mL of the metal colloids on coverslips used as sample holders.

2.2.3 ζ-Potential measurements. The determination of the colloidal stability was done using a Malvern Zetasizer Nano ZS (Malvern UK) in a 1 : 5 v/v dilution for the mono and bimetallic nanoparticles.

2.2.4 Scanning transmission electron microscopy. Scanning transmission electron microscopy (STEM) was used not only to determine the size and morphology of the Ag/Au NPs, but also to perform electron dispersive X-ray spectroscopy (EDX). The equipment used was an FEI Titan XFEG, equipped with a CEOS spherical aberration corrector for the electron probe, a Gatan Tridiem Energy Filter (GIF) and an Oxford X-ray spectrometer. Before electron microscopy observation, the samples were sonicated for several minutes, and few drops of the suspension were placed onto holey carbon copper microgrids. For every experiment, the aberrations were corrected using a gold standard sample assuring a spatial resolution of 0.8 Å.

2.2.5 X-ray photoelectron spectroscopy. Drops of the compounds dispersed in water were deposited on clean Si(100) substrates. After water evaporation the samples were loaded in vacuum load-lock chamber and then transferred in the XPS chamber. The XPS chamber has a base pressure of 10^{-10} mbar and is equipped with a hemispherical electron energy Analyzer (SPECS Phoibos 100 spectrometer) and an Al Kα (1486.29 eV) X-ray source. The angle between the hemispherical analyzer and the plane of the surface was kept at 60°. Wide scan spectra were recorded using an energy step of 0.5 eV and a pass-energy of 40 eV while specific core levels spectra (Ag 3d, O 1s, C 1s and Au 4f) were recorded using an energy step of 0.1 eV and a pass-energy of 20 eV. Data processing was performed with CasaXPS software (Casa software Ltd, Cheshire, UK). The absolute binding energies (BE) of the photoelectron spectra were determined by referencing the C–O component of the C 1s at 286.38 eV.[35] The contributions of the Al Kα satellite lines were subtracted, and the spectra were normalized to the maximum intensity.

2.3 Viability testing

2.3.1 Cell culture. To carry out the viability tests, peripheral blood mononuclear cells (PBMC) were obtained by mixing diluted blood (1 : 1 with saline) with Histopaque 1077 (Sigma, USA) and centrifuging at 400×*g* for 30 min at 25 °C. The PBMC layer was then harvested from the interface and washed twice with Hank's Balanced Salt Solution (HBSS) through centrifugation at 100×*g* for 10 min at 25 °C. After washing, the cells were resuspended in DMEM F-12. All procedures were performed under sterile conditions. The viability of the isolated blood cells was found to be over 90%, as determined by the Trypan blue exclusion test. To determine the cytotoxicity of the Ag/Au NPs, the MCF-7 human breast adenocarcinoma cell line was used. The MCF-7 cells were cultured in Dulbecco's Modified Eagle's Medium (DMEM, Gibco.) supplemented with 1% antibiotic–antimycotic and 10% fetal bovine serum (FBS) at 37 °C (5% CO_2 and 95% humidity). A total of 2.5×10^4 cells were grown in a 25 cm^2 flask until confluence.

2.3.2 Assessment of cell viability. MTT (3-(4,5-dimethylthiazol-2-yl)-2,5-diphenyltetrazolium bromide) (Sigma-Aldrich, St Louis, MO, USA) assay[36] was used to assess the cell viability of MCF-7 and PBMC cells exposed to different concentrations of mono- and bimetallic Ag/Au NPs at concentrations of 80–500 μM, *N*-acetyl-L-cysteine (NAC; Sigma-Aldrich, St Louis, MO, USA) and hydrogen peroxide (H_2O_2; Sigma-Aldrich, St Louis, MO, USA). The MCF-7 and PBMC cells were seeded at a density of 1×10^4 cells per well in 96-well culture plates for 24, 48 and 72 h. After culture, the medium in each well was replaced with a medium containing 10% MTT (5 mg mL^{-1} stock solution). After 4 h of incubation at 37 °C, the medium was removed and replaced with dimethyl sulfoxide (DMSO, Sigma-Aldrich, Steinheim, Germany) to dissolve purple formazan crystals. The optical density was read at 570 nm wavelength by the Elisa Reader (Biorad Hercules, California USA).

2.3.3 ROS production assay. To determine the ROS release, 1×10^5 MCF-7 cells were cultured in 12-well plates in the corresponding culture medium described previously. Cells were treated with Ag/Au NPs at concentrations of 180 μM, and using H_2O_2 (0.1% v/v) as positive control for 24 h. For ROS detection the Total ROS Assay Kit (ThermoFisher No. 88-5930-74) was used. Measurements were performed in plate-based assays using a fluorescent microplate reader at 495/520 nm.

2.3.4 ROS-dependent cell death induction and inhibition assay. To determine the inhibition of cell death in the MCF-7 human breast cancer cell line, we used NAC as a ROS inhibitor. The NAC was dissolved in deionized water and added to the MCF-7 cells 30 min before the 24 h-treatment with the Ag/Au NPs at concentrations of 180 μM. Once the treatment time was completed, ROS and MTT assays were performed to relate the cell viability with the presence or absence of ROS. Control experiments were conducted using H_2O_2 at CC_{50} doses as a ROS inducer and NAC as ROS inhibitor, as detailed in Section S1 (Fig. S1 and S2) in the ESI.†

2.3.5 Genotoxicity assay. To evaluate the possible DNA damage, 1×10^4 cells per well were seeded in a 24-well plate. After 24 h, the medium was replaced by 0.5 mL of medium with Ag/Au NPs at concentrations of 180 μM. The negative control was represented by MCF-7 cells cultivated in an NP-free growth medium by 24 h incubation, the control positive was represented using etoposide (20 μM) for 4 h. After this step, the cells were removed from the wells by using trypsin/EDTA solution and centrifuged for 2 min at 700 g. Finally, cells with a density of 10^6 cells per mL were suspended in cold PBS (without Mg^{2+} and Ca^{2+}) and the cell DNA damage was measured using alkaline comet assay according to the supplier's instructions (OxiSelect TM Comet Assay Kit, CELL BIOLABS, INC). Each sample was analyzed by CASPlab software. In this study, the mean of "percentage of DNA in the tail and olive tail moment" was used and reported as the amount of DNA damage.

2.3.6 Statistical analysis. All the biological experiments were done in triplicate, and the results were assessed for statistical significance using a two-way ANOVA and Tukey's test ($p < 0.05$ is considered significant), using GraphPad Prism 7.00 software.

3 Results

3.1 Characterization of the Ag/Au NPs

Green synthesis of colloidal gold (Au NPs), silver (Ag NPs) and silver/gold (Ag/Au NPs) nanoparticles was carried out by a wet chemical reduction of the respective ions (Ag^+ and $AuCl_4^-$) using water-soluble starch as both reducing and coating agent.[37] Regarding the possible application of noble metal NPs in nanomedicine, it is essential to guarantee the dispersibility of the NPs in water and, therefore, in the cell culture media. For this purpose, the coating agent must be hydrophilic in nature and, most importantly, biocompatible,[38] all these requirements are met by starch. The optical properties of the Ag/Au NPs were characterized by UV-vis spectroscopy. All the absorption spectra of the metal colloids presented a single absorption band related to the localized surface plasmon resonance (LSPR)[37] (Fig. 1A).

The dependence of the wavelength (λ) at the maximum absorbance as a function of NP composition is depicted in Fig. 1B. The bathochromic shift is attributed to the presence of the two elements at different chemical compositions.[37] The PXRD patterns of the Ag/Au NPs are shown in Fig. 1C, which confirms their crystalline nature. The diffraction peaks observed at $2\theta = 38.3$, 44.5, 64.8, 77.8 and 81.8° correspond to the (111), (200), (220), (311) and (222) crystallographic planes, respectively, for bulk face-centered cubic (FCC) Au and Ag.[39] Additionally, the ζ-potential values of the colloidal Ag/Au NPs were considered to evaluate the stability of the colloids. In general, a colloid or suspension is considered stable if the ζ-potential value is above a critical value of ± 30 mV.[39] According to the measured ζ-potential values for the colloidal Ag/Au NPs, *i.e.*, between −21.2 and −32.8 mV (Fig. 1D), our starch-capped Ag/Au NPs colloids can be considered relatively stable in water.

In Fig. 2, low-magnification Cs-corrected STEM-HAADF images of the mono- and bimetallic Ag/Au NPs are presented. It can be observed that the NPs are quasi-spherical in shape, where facets can be also identified, with particle sizes ranging from 10 to 30 nm. It is important to highlight that in many cases the NPs were connected forming a chain-like structure except for the Au NP system. A closer examination revealed that the NPs are multi-twinned (Fig. S3†), which is prevalent in many similar colloidal NP systems.[40,41] Additionally, for the Ag system, it was observed small clusters (below than 1 nm) pending from the nanoparticles probably due to the remaining AgCl formed from the Ag and Au precursors that did not completely react, an effect that was not present in any other system that displayed "cleaner" surfaces.

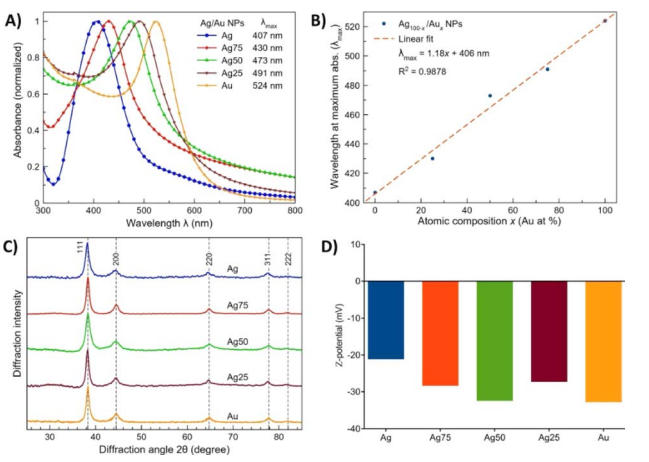

Fig. 1 Characterization of the Ag/Au NPs. (A) Absorption spectra in the UV-vis region. (B) Dependence of the wavelength at the maximum absorbance (λ_{max}) as a function of NP chemical composition. (C) PXRD patterns. Dotted lines indicate the expected position for (FCC) Au.[39] (D) ζ-potential values of the colloids.

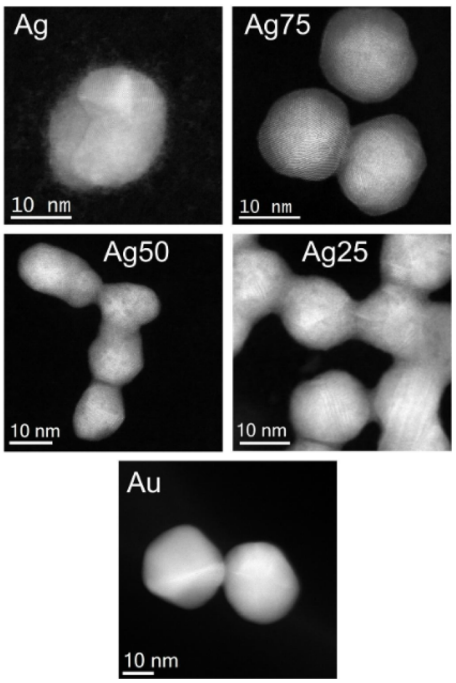

Fig. 2 Cs-corrected STEM-HAADF analysis of the mono- and bimetallic Ag/Au nanoparticles.

The EDS mapping analysis. Fig. 3, revealed a relatively homogeneous distribution of the Ag and Au elements in the bimetallic nanoparticles. Noteworthy to mention is that the high Ag-content bimetallic nanoparticles (Ag75) present a core–shell type structure, with an Au rich core and an Ag rich shell, as previously reported.[37] The expected and experimental chemical compositions of the bimetallic nanoparticles determined by the EDS and XPS (*vide infra*) analysis is presented in Table 2, where the experimental values are relatively close to the targeted compositions.

3.2 XPS results

The Ag/Au NPs samples were analyzed by XPS. Table S1† presents the composition of the samples extracted from the analysis of the wide energy range scans. All the samples presented carbon (C) and oxygen (O) from the starch acting as capping agent and silicon (Si) from the substrates used. In addition, most of the samples presented traces of nitrogen (N) and chlorine (Cl), probably from the Ag and Au precursors. The amount of Ag and Au detected in each sample is in good agreement with the expected nominal atomic ratio (Ag : Au)

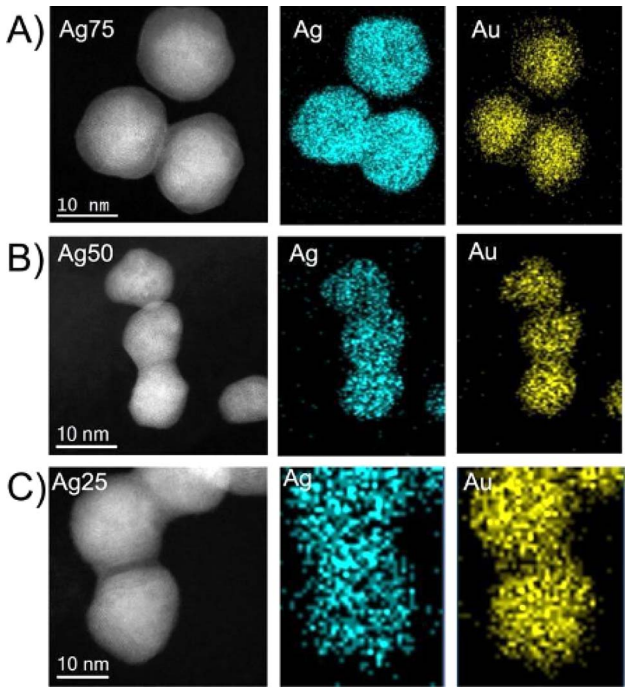

Fig. 3 EDS elemental mapping of the bimetallic Ag/Au NPs with different Ag : Au atomic ratio. (A) Ag75; (B) Au50; (C) Ag25.

Table 2 Comparison between the expected and experimental chemical compositions of the bimetallic Ag/Au NPs

	Expected	Experimental EDS	Experimental XPS
System	Ag : Au ratio	Ag : Au ratio	Ag : Au ratio
Ag	N/A	N/A	N/A
Ag75	3	3.16	2.8
Ag50	1	0.90	1.2
Ag25	0.33	0.37	0.6
Au	N/A	N/A	N/A

except for the Ag25 sample, which has a larger proportion of Ag than expected, as observed in Table 2.

Fig. 4A displays the analysis of the Ag 3d core level peaks of the samples. Depending on the nanoparticle composition, there are some differences among them. The first one is the relative positioning of the bands with respect to the bulk Ag (368.3 eV).[42] The corresponding signal for Ag NPs is shifted towards lower binding energies (BE) while the alloyed Ag/Au NPs presented positive shifts up to 0.2 eV as shown in Fig. S4,† following a similar trend as the one previously reported for Ag/Au NPs.[37] It is well-known that the BE position of the Ag 3d peak in monometallic (Ag NPs) and bimetallic Ag/Au NPs depends not only on the stoichiometry, but also on the NP size and density.[43] However, there is not a clear agreement in the literature concerning the origin of this shift and, for Ag NPs, it has been reported either an increase[44] or a decrease[45] of the BE with the increasing NP size.

In our case, the lack of a clear correlation between the observed BE shift and stoichiometry of the NPs can be ascribed

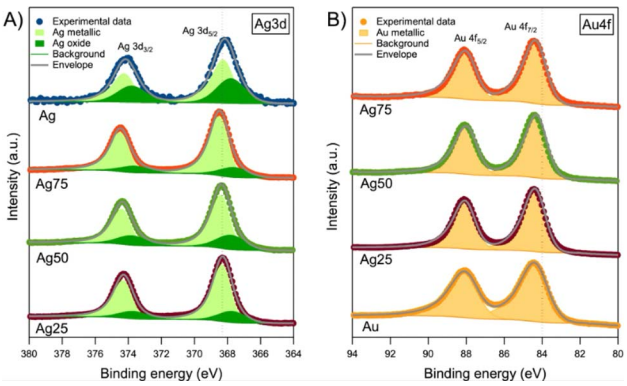

Fig. 4 XPS core level spectra of (A) Ag 3d and (B) Au 4f of the Ag/Au NPs. Dashed lines represent the BE of Ag and Au bulk, respectively.

to the different NP sizes. For the fine analysis of the Ag 3d core level spectra (Fig. 4A), two components were used for the fitting. First, there is a main component at 368.4 ± 0.1 eV, which includes either pure Ag or Ag/Au alloy. Both contributions are not easily distinguished, especially at the nanoscale, due to the already mentioned size effects.

Second, there is an additional component at lower BE (367.7 ± 0.1 eV) that corresponds to oxidized Ag (*i.e.*, Ag^{+} or Ag^{2+}). Usually, this BE value is related to Ag_2O.[46] However, considering the shifts observed in the main component (either as pure Ag or Ag/Au alloy), we decided to evaluate the BE shift between metallic and oxide components to elucidate the oxide present in the NPs. According to Weaver and Hoflund,[46] these BE shifts are −0.7 eV for AgO and −0.3 eV for Ag_2O in powders. In our case, the shifts registered are intermediate between the two oxides (−0.5 eV) and, therefore, the presence of both oxides cannot be ruled out. The only exception is the Ag75 sample, whose BE shift is even larger than the one reported for AgO. In this case, we assumed that the oxide present is AgO. Moreover, Fig. 4B displays the Au 4f core level peaks of the NPs. In this analysis, a single component was necessary to perform the fitting at 84.4 ± 0.1 eV. As occurred in the analysis of the Ag 3d core level, the NPs presented a shift with respect to bulk Au (84.0) eV.[42] Further analysis about the XPS core level spectra of C 1s and O 1s is found in Section S3 and Fig. S5.†

3.3 Cell viability studies

The metabolic activity of MCF-7 (breast cancer cell model) and PBMC (healthy cell model) cells treated with different concentrations of Ag/Au NPs (*i.e.*, 80–500 μM) was measured for 24 h by MTT assay, and the results are summarized in Fig. 5. For MCF-7 cells (Fig. 5A), the NP concentration-dependence of the cell viability is closely related to the type of the Ag/Au NPs. For example, for Ag, Ag75, Ag25 and Au NPs, the cell viability tends to decrease starting at the initial NP concentration of 80 μM, whereas for Ag50 NPs the decrease trend is initiated at 100 μM. From the concentration of 300 to 500 μM, the monometallic Ag NPs showed to be more cytotoxic than the Au NPs and the bimetallic ones. Furthermore, it was demonstrated that whereas the mono- and bimetallic Ag/Au NPs induced certain

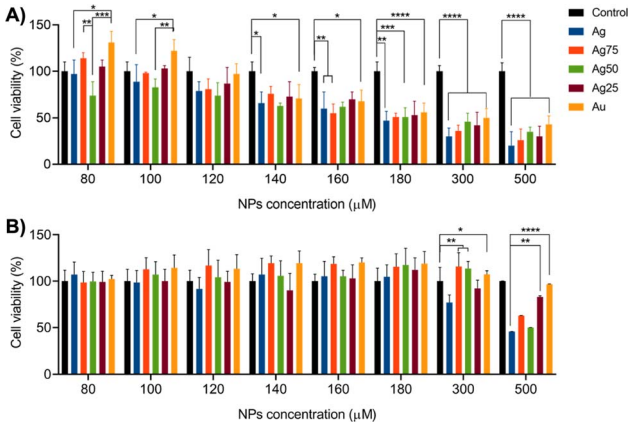

Fig. 5 Cytotoxic studies of the Ag/Au NPs upon 24 h treatment on (A) MCF-7 cancer cells and (B) healthy PBMC. *$p < 0.05$, **$p < 0.01$, ***$p < 0.001$ and ****$p < 0.0001$. Abbreviation: PBMC: peripheral blood mononuclear cells. Control: cells cultured only with culture medium.

concentration-dependent cell death in MCF-7 cancer cells, the cell viability of healthy PBMCs was not severely affected by the treatments until the NP concentration reached 500 μM (Fig. 5B). These assays proved to be useful in determining the cytotoxic concentration 50% (CC_{50}) and the effective concentration 50% (EC_{50}) values of the Ag/Au NPs, which are the NP concentrations needed to reduce the cell viability of the MCF-7 (cancer cells) and PBMC (healthy cells), respectively, by 50% (Table 3). To compare objectively if the CC_{50} values of the metallic NPs against MCF-7 cancer cells of the different nanosystems are relatively low or high, we calculated the therapeutic index (TI) that compares the NP concentration at which the treatment becomes cytotoxic against healthy PBMCs and the concentration at which the drug is effective against MCF-7 cancer cells. The larger the value of TI, the safer the treatment is. In our case, we obtained TI values from 4.2 for the Ag NPs to 10.5 for Au NPs. These results demonstrate the potential application of the Ag/Au NPs as therapeutic agents against MCF-7 cancer cells. Additionally, the MCF-7 cells were treated with the Ag/Au NPs at exposure times of 48 and 72 h (Fig. S6†). In both cases, a NP concentration-dependent decrease of the cell viability was observed and the Ag NPs showed to be more cytotoxic compared to the rest of the nanosystems, as was observed in the cytotoxic study done at 24 h of treatment. In order to normalized the comparative biological studies presented further, we decided to used a NP concentration of 180 μM for all the five nanosystems.

Table 3 Therapeutic index (TI) values of mono- and bimetallic Ag/Au nanoparticles

System	CC_{50} (μM)	EC_{50} (μM)	TI
Ag	891.0	212.5	4.2
Ag75	1289.4	237.0	5.4
Ag50	1128.5	255.8	4.4
Ag25	2655.0	263.5	10.1
Au	3189.3	304.7	10.5

It has been demonstrated that the cytotoxicity of metal nanoparticles depends on their shape, surface, size, and chemical composition.[47,48] Regarding the cytotoxic effect of bimetallic Ag/Au NPs, it has been reported that the combination of Ag with other noble metals, such Au, promotes an improvement in antitumor activity. For example, green synthesized Ag/Au NPs, in similar concentrations, may exhibit lower cytotoxic activity against healthy human cells (human dermal fibroblast) than the one against cancerogenic cells (melanoma).[34]

In other examples, Ag/Au NPs with compositions of Ag50 were synthesized using *Stigmaphyllon ovatum* extracts showing antitumor activity against HeLa cells.[49] Adeyemi, *et al.* used *Dovyalis caffra* extracts in the synthesis of Ag/Au NPs showing antitumor activity against MCF-7 cells for which CC_{50} values of 77.6 μM were reported.[50] Furthermore, the cytotoxic effect of bimetallic Ag/Au NPs has also been reported in the evaluation of acute toxicity in *Daphnia magna*. It was reported that Ag/Au NPs with Ag : Au atomic ratios of 80 : 20 and 20 : 80 showed similar results without significant differences, *i.e.*, the CC_{50} was around 12–15 μg L^{-1} for both nanosystems.[51]

3.4 Ag/Au NPs induce ROS production and ROS-dependent cell death in MCF-7 cells

To determine if ROS production was the main cytotoxic mechanism induced by the Ag/Au NPs in MCF-7 cells two different types of experiments were carried out: (i) ROS production assays and (ii) ROS-dependent cell death induction and inhibition tests. The ROS production assays were done by fluorescence staining tests, while the inhibition experiments were done using NAC as ROS inhibitor (Fig. 6). It was found that the treatment of MCF-7 cells with Ag/Au NPs at concentrations of 180 μM induced ROS production in the cells (Fig. 6A and B). The NPs with a higher proportion of Ag, mainly the samples Ag, Ag75 and Ag50, showed a greater production of ROS. These results were corroborated by fluorescence microscopic images (Fig. 6B).

To corroborate further that the cell death of the human breast cancer MCF-7 cells induced by the Ag/Au NPs was *via* the production of ROS, we pre-treated the cancer cells with NAC, a synthetic precursor of intracellular cysteine and glutathione (GHS) and, consequently, an important antioxidant.[52] As a first approach, we determined the NAC concentration needed to recover the cell viability of MCF-7 cells treated with H_2O_2 (used as endogenous ROS)[53] at a CC_{50} dose of 0.1% v/v (Fig. S1A and S2†). According to these experiments, a NAC concentration of 5 mM was enough to get a cell viability recovery of around 70–80% (Fig. S2†). Important to notice is that this NAC concentration did not have any effect on the MCF-7 cell viability (Fig. S1B†). The effect of NAC pretreatment on MCF-7 cells treated with Ag/Au NPs for 24 h can be evaluated in the experiments related to the decrease in ROS production according to fluorescence detection tests, as seen in Fig. 6A and B. The decrease of the ROS production was observed preferentially in the NPs with a higher Ag concentration (Ag, Ag75 and Ag50 NPs). The action of NAC results from the elimination of free radicals and the increase in intracellular GSH levels.[52] In the

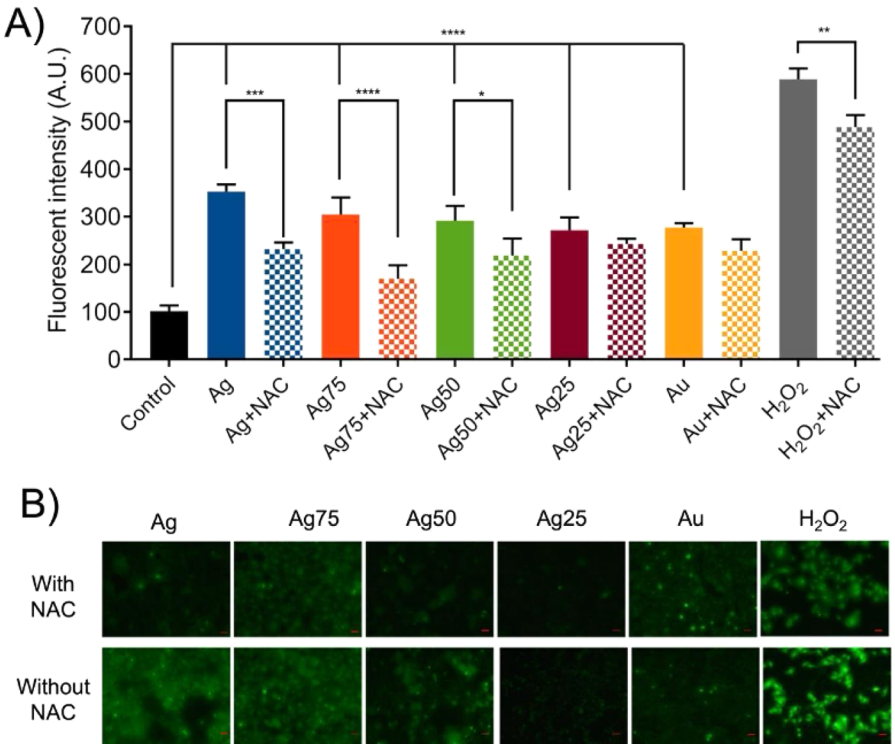

Fig. 6 ROS production in MCF-7 cells upon treatment with Ag/Au NPs at concentrations of 180 μM and H_2O_2 at 0.1% v/v as a positive control with and without NAC (5 mM) pretreatment for 24 h. (A) ROS fluorescence intensity; (B) fluorescence microscopic images of ROS production. Control: cells cultured only with culture medium. Scale bar: 5 μm. *p < 0.05 **p < 0.01, ***p < 0.001 and ****p < 0.0001.

cases of the nanosystems based on Ag25 and Au NPs, it seems to be that NAC-pretreatment did not significantly influence the reduction of ROS production. So far, we do not have a plausible explanation for these observations, meaning that these nanosystems should be further studied to understand the type of cell death mechanism that they induce in the MCF-7 cancer cells. Consequently, the highest levels of recovery of the cell viability for MCF-7 with a NAC-pretreatment was observed for treatments with Ag, Ag75 and Ag50 NPs, *i.e.*, around 20–30% of recovery (Fig. 7). Surprisingly, a relatively high cell viability recovery (around 20%) was observed for the MCF-7 cancer cells treated with Au NPs and pretreated with NAC. Previous investigations suggest that cancer cells are more susceptible to electron transfer between bimetallic NPs, which release ROS[25] that promotes cell death in different types of cancer cell lines, for example in breast cancer cells (MCF-7),[54] lung cancer (A549),[27] leukemia (Jurkat, human T lymphocyte cells),[55] human colon cancer (HT-29), cervical cancer (HeLa)[56] and human bladder cancer (T24).[25,54]

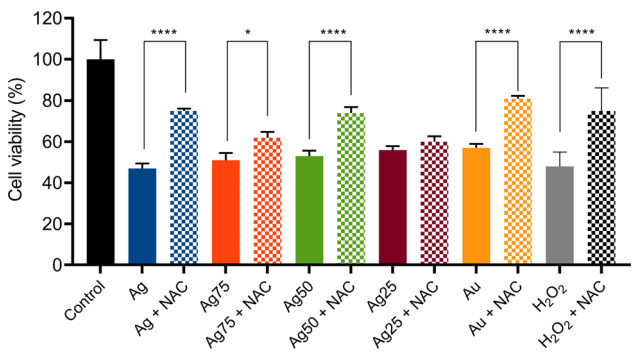

Fig. 7 ROS-dependent cytotoxic effect of bimetallic Ag/Au NPs at concentrations of 180 μM and H_2O_2 at 0.1% v/v on the cell viability of MCF-7 cells with and without NAC (5 mM) pretreatment. Control: cells cultured only with culture medium. *p < 0.05, **p < 0.01, ***p < 0.001 and ****p < 0.0001.

Moreover, oxidative stress within the cells is considered as one of the primary mechanisms underlying the NP antitumor activity.[31] For instance, Ag and Au NPs were reported to have an intrinsic property that allows a Fenton-type reaction to produce ROS[57] with a subsequent lipid and protein oxidation, DNA damage, and cell death.[24,58] Therefore, our results indicate that the bimetallic Ag/Au NPs induced the production of intracellular ROS in tumor cells being the principal toxic source, mainly in the NPs that present a greater amount of Ag, although it has also been reported that Au NPs can present this death mechanism.[59–61] These results correlate well with cytotoxicity studies of nanomaterials, where the production of ROS is the main mechanism associated with regulated cell death.[62]

3.5 Genotoxicity assessment using a mini-gel comet assay

As mentioned previously, several studies suggest that the cytotoxicity of NPs depends on ROS production,[37,54,58,63–65] which generates oxidative stress in the cell that leads to a depolarization of the mitochondria, damage to proteins, lipids and/or DNA.[31] To determine the possible origin of the ROS generated

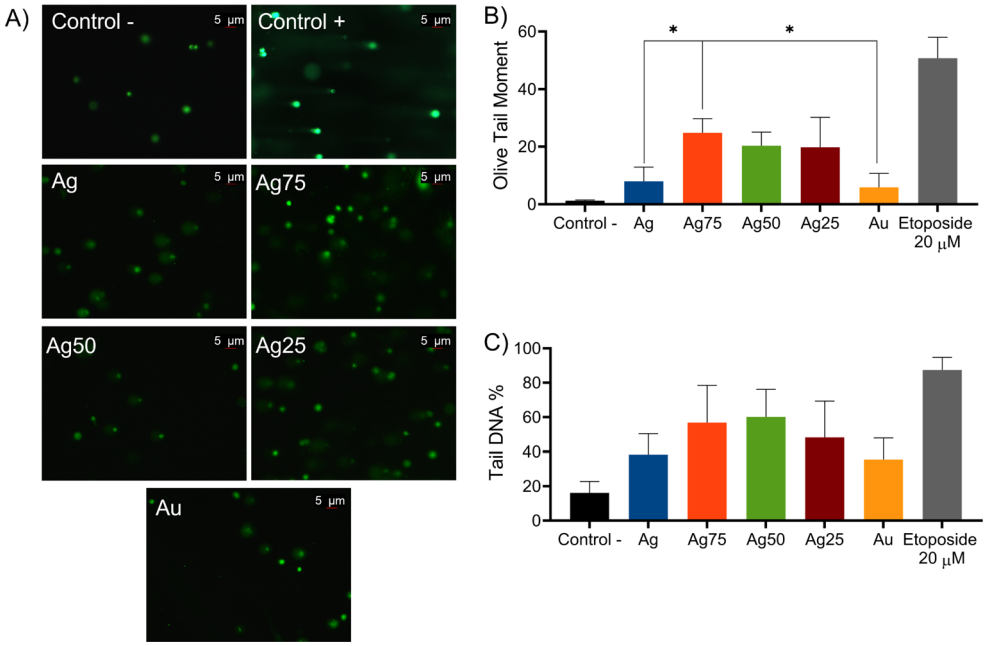

Fig. 8 Comet parameters observed in (A) comet images, (B) olive tail moment (C) and tail DNA%. Control: cells cultured only with culture medium. *$p < 0.05$.

by the presence of Ag/Au NPs in MCF-7 cancer cells, we used the comet assay method to assess DNA damage. This method, also known as single-cell gel electrophoresis, can detect single and double-strand DNA breaks, as well as alkaline labile sites. The damage of DNA is reflected by the increase in the comet parameter, *i.e.*, DNA percentage in tail and olive tail moment.[66] Our study reports the damage of DNA induced by bimetallic Ag/Au NPs in the formation of comets (Fig. 8A), and the increase of the DNA tail moment (Fig. 8B). The DNA damage was higher in the Ag75 NPs with 24%, showing significant differences compared to the monometallic ones (Fig. 8B) and considering the parameter of the percentage of the tailed DNA (tail DNA%), the Ag75 and Ag50 NPs showed a greater fragmentation of the DNA present in the tail (Fig. 8C). However, no differences were found between groups of bimetallic Ag/Au NPs.

In any case, these results resemble those reported by Lebedová *et al.*, demonstrating that Ag NPs showed a more significant genotoxic effect on HBEC cells than Au NPs.[60] The same effect was observed in fibrosarcoma cells, as reported by Sivakumar *et al.*, where Ag NPs showed the highest genotoxic effect.[67] The genotoxic effect of Ag75 NPs has been assessed in Sprague Dawley rats by administering a single dose of 5 mg kg^{-1} IV, where most of the Ag/Au NPs were rapidly eliminated from the circulatory system. However, a small concentration (2.97 ± 0.05 g/100 g) retained in the liver caused genotoxicity after 14 days.[68]

Taking into consideration our results, we can conclude that bimetallic starch-stabilized Ag/Au NPs, having a relatively high Ag content, generate cytotoxicity through the increase in the production of ROS that causes DNA damage in human breast cancer MCF-7 cells. Although more studies are needed to establish a more complete pathway of cell death induced by these NPs, considering other organelles such as mitochondria or endoplasmic reticulum present in cancer cells.

4 Conclusions

In this work, we report the synthesis of colloidal bimetallic Ag/Au nanoparticles using starch as a reducing and capping agent with different and controllable atomic proportions of Ag and Au. Furthermore, the anticancer therapeutic potential of the NPs was tested in human breast cancer MCF-7 cells, showing a significant cytotoxic activity at 180 μM, but negligible cytotoxicity in PBMC cells at the same concentrations. At the same dose, the NPs induced a ROS-dependent cell death, where the bimetallic Ag/Au NPs affected the stability of nuclear DNA of the MCF-7 cancer cells. Specifically, the Ag75 and Ag50 NPs presented the highest anticancer activity in terms of ROS production and DNA damage.

Finally, this work opens the door to evaluate in more detail the importance of the composition of bimetallic nanoparticles based on noble metals in the cytotoxicity mechanism, which could contribute to their widespread use and clinical application.

Data availability

Data for this article, including XPS, XRD, UV-vis spectroscopy, zeta-potential, and cell viability data are available at Digital CSIC at **https://doi.org/10.20350/digitalCSIC/16703**.

Author contributions

Conceptualization, J. J. M. S. and J. L. C. D.; methodology, J. J. M. S. and J. L. C. D.; validation, J. J. M. S. and M. P. G. G.;

investigation, J. J. M. S., M. P. G. G., A. M., L. M. and Y. H., writing – original draft preparation, J. J. M. S., L. M. and Y. H.; writing – review and editing, J. J. M. S., D. Z. T., M. P. G. G., J. M. G. M., A. M., L. M., Y. H. and J. L. C. D.; visualization, J. J. M. S., M. P. G. G., J. M. G. M., A. M., L. M., Y. H. and J. L. C. D.; supervision, J. L. C. D.; project administration, J. J. M. S. and J. L. C. D.; funding acquisition, L. M. and J. L. C. D. All authors have read and agreed to the published version of the manuscript.

Conflicts of interest

There are no conflicts to declare.

Acknowledgements

The authors thank Anna Valeria Ortega Perez for providing the PXRD measurements. The groups at CSIC and Tecnologico de Monterrey acknowledge the Acciones Bilaterales de Movilidad Conjunta, Modalidad B, program (ref. BILTC22001) for financial support. The group at Tecnologico de Monterrey thanks the School of Engineering and Sciences at Tecnologico de Monterrey for partial funding provided through the Research Chair of Photonics and Quantum Systems and the Department of Science at Tecnologico de Monterrey for access to laboratories and characterization equipment. Authors acknowledge the use of instrumentation as well as the technical advice provided by the National Facility ELECMI ICTS node "Laboratorio de Microscopías Avanzadas" at the University of Zaragoza. Y. H., L. M. and J. M. G.-M. acknowledge the financial support of the Spanish Ministry of Science and Innovation to grant PID2021-126524NB-100 funded by MCIN/AEI/10.13039/501100011033 and by "ERDF A way of making Europe". AM acknowledges the Spanish Ministry of Science and Innovation (RYC2018-024561-I), the Gobierno the Aragon (Nanomidas group, code E13-23R) and the grant CEX2023-001286-S funded by MICIU/AEI/10.13039/501100011033.

Notes and references

1 H. Sung, J. Ferlay, R. Siegel, M. Laversanne, I. Soerjomataram, A. Jemal and F. Bray, *CA: Cancer J. Clin.*, 2020, **71**, 209–249.
2 L. Wilkinson and T. Gathani, *Brit. J. Radiol.*, 2022, **95**, 20211033.
3 L. Torre, F. Bray, R. Siegel, J. Ferlay, J. Lortet-Tieulent and A. Jemal, *CA: Cancer J. Clin.*, 2015, **65**, 87–108.
4 **https://www.who.int/es/news-room/fact-sheets/detail/breast-cancer**.
5 N. Azamjah, Y. Soltan-Zadeh and F. Zayeri, *Asian Pac. J. Cancer Prev.*, 2019, **20**, 87–108.
6 I. Mittra, G. A. Mishra, R. P. Dikshit, S. Gupta, V. Kulkarni, H. Shaikh, S. Shastri, R. Hawaldar, S. Gupta, C. S. Pramesh and R. A. Badwe, *BMJ*, 2021, **372**(256), 1–9.
7 V. Sopik, *Breast Cancer Res. Treat.*, 2021, **186**(2), 497–507.
8 A. M. Gonzalez-Angulo, F. Morales-Vasquez and G. N. Hortobagyi, *Adv. Exp. Med. Biol.*, 2007, **608**, 1–22.
9 L. Galluzzi, J. Bravo-San Pedro and I. E. A. Vitale, *Cell Death Differ.*, 2015, **22**, 58–73.
10 J. Ben-Dror, M. Shalamov and A. Sonnenblick, *Genes*, 2022, **960**, 209–249.
11 K. P. Trayes and S. E. H. Cokenakes, *Am. Fam. Physician*, 2021, **104**, 171–178.
12 K. Fabian, J. Kowalczyk, S. Reynolds and J. Hodge, *Cells*, 2022, **3**, 3826.
13 R. Sakthi Devi, A. Girigoswami, M. Siddharth and K. Girigoswami, *Appl. Biochem. Biotechnol.*, 2022, **194**, 4187–4219.
14 M. Ashrafizadeh, A. Zarrabi, A. Bigham, A. Taheriazam, Y. Saghari, S. Mirzaei, M. Hashemi, K. Hushmandi, H. Karimi-Maleh, E. Nazarzadeh Zare, E. Sharifi, Y. N. Ertas, N. Rabiee, G. Sethi and M. Shen, *Med. Res. Rev.*, 2023, **43**, 2115–2176.
15 Z. Mirza and S. Karim, *Semin. Cancer Biol.*, 2021, **69**, 226–237.
16 M. Salimi, S. Sarkar, R. Saber, H. Delavari, A. M. Alizadeh and H. T. Mulder, *Cancer Nanotechnol.*, 2018, **9**, 7.
17 R. Sakthi Devi, A. Girigoswami, M. Siddharth and K. Girigoswami, *Appl. Biochem. Biotechnol.*, 2022, **194**, 4187–4219.
18 L. Liu, Y. Wang, L. Miao, Q. Liu, S. Musetti, J. Li and L. Huang, *Mol. Ther.*, 2018, **26**, 45–55.
19 F. Huang, N. Pan, Y. Wei, J. Zhao, M. Aldarouish, X. Wang, X. Sun, Z. Wen, Y. Chen and L. Wang, *Front. Immunol.*, 2021, **12**, 707298.
20 K. de Oliveira Gonçalves, D. Vieira, D. Levy, S. P. Bydlowski and L. C. Courrol, *Carbohydr. Res.*, 2020, **32**, 102080.
21 A. M. Aly Khalil, E. Saied, A. Mekky, A. M. Saleh, O. Al Zoubi and A. Hashem, *Front. Bioeng. Biotechnol.*, 2024, **11**, 1294170.
22 H. Katifelis, I. Mukha, P. Bouziotis, N. Vityuk, C. Tsoukalas, A. Lazaris, A. Lyberopoulou, G. Theodoropoulos, E. P. Efstathopoulos and M. Gazouli, *Int. J. Nanomed.*, 2020, **15**, 6019–6032.
23 H. Nosrati, Y. Baghdadchi, R. Abbasi, M. Barsbay, M. Ghaffarlou, F. Abhari, A. Mohammadi, T. Kavetskyy, S. Bochani, H. Rezaeejam, S. Davaran and H. Danafar, *J. Mater. Chem. B*, 2021, **9**, 4510–4522.
24 I. Shmarakov, I. Mukha, N. Vityuk, V. Borschovetska, N. Zhyshchynska, G. Grodzyuk and A. Eremenko, *Nanoscale Res. Lett.*, 2017, **12**, 1–10.
25 L. Berta, N. A. Coman, A. Rusu and C. Tanase, *Materials*, 2021, **14**, 7677.
26 D. Sharma, L. Ledwani, N. Kumar, T. Mehrotra, N. Pervaiz and R. Kumar, *Arabian J. Sci. Eng.*, 2021, **46**, 275–285.
27 S. A. Fahmy, I. M. Fawzy, B. M. Saleh, M. Y. Issa, U. Bakowsky and H. M. E. Azzazy, *Nanomaterials*, 2021, **11**, 965.
28 S. Ali, A. Sharma, W. Ahmad, M. Zareef, M. Hassan, A. Viswadevarayalu, T. Jiao, H. Li and Q. Chen, *Crit. Rev. Anal. Chem.*, 2021, **51**, 454–481.
29 E. Eruslanov and S. Kusmartsev, *Methods Mol. Biol.*, 2010, **594**, 57–72.
30 I. Dalle-Donne, D. Giustarini, R. Colombo, R. Rossi and A. Milzani, *Trends Mol. Med.*, 2021, **9**, 169–176.
31 M. Schieber and N. S. Chandel, *Curr. Biol.*, 2014, **24**, R453–R462.

32 A. Manke, L. Wang and Y. Rojanasakul, *BioMed Res. Int.*, 2013, **2013**, 942916.
33 X. Zhao, T. Qi, C. Kong, M. Hao, Y. Wang, J. Li, B. Liu, Y. Gao and J. Jiang, *Int. J. Nanomed.*, 2018, **13**, 6413–6428.
34 D. Lomelí-Marroquín, D. Medina Cruz, A. Nieto-Argüello, A. Vernet Crua, J. Chen, A. Torres-Castro, T. J. Webster and J. L. Cholula-Díaz, *Int. J. Nanomed.*, 2019, **14**, 2171–2190.
35 H. Hantsche, *Adv. Mater.*, 1993, **5**, 778.
36 T. Mosmann, *J. Immunol. Methods*, 1983, **65**, 55–63.
37 A. Nieto-Argüello, D. Medina-Cruz, Y. S. Pérez-Ramírez, S. Pérez-García, M. A. Velasco-Soto, Z. Jafari, I. De Leon, M. González, Y. Huttel, L. Martínez, A. Mayoral, T. J. Webster, J. M. García-Martín and J. L. Cholula-Díaz, *Nanomaterials*, 2022, **12**, 779.
38 B. Klębowski, J. Depciuch, M. Parlińska-Wojtan and J. Baran, *Int. J. Mol. Sci.*, 2018, **19**, 4031.
39 I. K. Suh, H. Ohta and Y. Waseda, *J. Mater. Sci.*, 1988, **23**, 757–760.
40 J. S. Du, W. Zhou, S. M. Rupich and C. A. Mirkin, *Angew. Chem.*, 2021, **133**, 6934–6939.
41 M. Song, G. Zhou, N. Lu, J. Lee, E. Nakouzi, H. Wang and D. Li, *Science*, 2020, **367**, 40–45.
42 *Physical Electronics Division*, ed. C. D. Wanger, W. M. Riggs, L. E. Davis, J. F. Moulder and G. E. Muilenberg, Wiley, Eden Prairie, Minnesota, USA, 3rd edn, 1981.
43 L. Martinez, M. Diaz, E. Roman, M. Ruano, D. Llamosa P and Y. Huttel, *Langmuir*, 2012, **28**, 11241–11249.
44 I. Lopez-Salido, D. C. Lim and Y. D. Kim, *Surf. Sci.*, 2012, **588**, 6–18.
45 M. Schnippering, M. Carrara, A. Foelske, R. Kötz and D. J. Fermín, *Phys. Chem. Chem. Phys.*, 2007, **9**, 725–730.
46 J. Weaver and G. Hoflund, *J. Phys. Chem.*, 1994, **98**, 8519–8524.
47 A. Woźniak, A. Malankowska, G. Nowaczyk, B. Grześkowiak, K. Tuśnio, R. Słomski, A. Zaleska-Medynska and S. Jurga, *J. Mater. Sci.*, 2017, **28**, 8519–8524.
48 A. Chompoosor, K. Saha, P. S. Ghosh, D. J. Macarthy, O. R. Miranda, Z. J. Zhu, K. F. Arcaro and V. M. Rotello, *Small*, 2010, **6**, 2246–2249.
49 E. E. Elemike, D. C. Onwudiwe, N. Nundkumar, M. Singh and O. Iyekowa, *Mater. Lett.*, 2019, **243**, 148–152.
50 J. O. Adeyemi, E. E. Elemike, D. C. Onwudiwe and M. Singh, *Inorg. Chem. Commun.*, 2019, **109**, 107569.
51 T. Li, B. Albee, M. Alemayehu, R. Diaz, L. Ingham, S. Kamal, M. Rodriguez and S. W. Bishnoi, *Anal. Bioanal. Chem.*, 2019, **398**, 689–700.
52 S. Y. Sun, *Cancer Biol. Ther.*, 2010, **9**(2), 109–110.
53 D. R. Gough and T. G. Cotter, *Cell Death Dis.*, 2011, **2**, 213.
54 J. O. Unuofin, A. O. Oladipo, T. A. Msagati, S. L. Lebelo, S. Meddows-Taylor and G. K. More, *Arabian J. Chem.*, 2020, **13**, 6639–6648.
55 R. Dobrucka, A. Romaniuk-Drapała and M. Kaczmarek, *Biomed. Microdevices*, 2020, **22**, 1–11.
56 G. Thirumoorthy, B. Balasubramanian, J. A. George, A. Nizam, P. Nagella, N. Srinatha, M. Pappuswamy, A. M. Alanazi, A. Meyyazhagan, K. R. R. Rengasamy and V. Veerappa Lakshmaiah, *Sci. Rep.*, 2024, **14**, 1270.
57 S. Navalon, M. de Miguel, R. Martin, M. Alvaro and H. Garcia, *J. Am. Chem. Soc.*, 2011, **133**, 2218–2226.
58 D. Dutta, A. K. Sahoo, A. Chattopadhyay and S. S. Ghosh, *J. Mater. Chem. B*, 2016, **4**, 793–800.
59 Q. Xia, H. Li, Y. Liu, S. Zhang, Q. Feng and K. Xiao, *J. Biomed. Mater. Res., Part A*, 2017, **105**, 710–719800.
60 J. Lebedová, Y. S. Hedberg, I. Odnevall Wallinder and H. L. Karlsson, *Mutagenesis*, 2018, **33**, 77–85.
61 A. Avalos, A. I. Haza, D. Mateo and P. Morales, *Food Chem. Toxicol.*, 2018, **120**, 81–88.
62 P. P. Fu, Q. Xia, H. M. Hwang, P. C. Ray and H. Yu, *J. Food Drug Anal.*, 2014, **22**, 64–75.
63 K. Kang, H. Jung and J. S. Lim, *Biomol. Ther.*, 2012, **20**, 399.
64 N. M. Schaeublin, L. K. Braydich-Stolle, A. M. Schrand, J. M. Miller, J. Hutchison, J. J. Schlager and S. M. Hussain, *Nanoscale*, 2011, **3**, 410–420.
65 X. Lu, T. Mei, Q. Guo, W. Zhou, X. Li, J. Chen, X. Zhou, N. Sun and Z. Fang, *Microchim. Acta*, 2019, **186**, 1–7.
66 M. Glei, T. Schneider and W. Schlörmann, *Arch. Toxicol.*, 2016, **90**, 2315–2336.
67 A. Sivakumar, C. Krishnaraj, S. Sheet, D. Rampa, D. Kang, S. Belal, A. Kumar, I. Hwang, S. Yun, Y. Lee and K. Shim, *In Vitro Cell. Dev. Biol.*, 2017, **53**, 632–645.
68 D. Wang, M. Dan, Y. Ji, X. Wu, L. Xu and H. Wen, *J. Biomed. Nanotechnol.*, 2018, **14**, 1953–1964.